

The creation of two-dimensional composite solitons in spin-orbit-coupled self-attractive Bose-Einstein condensates in free space

Hidetsugu Sakaguchi and Ben Li

*Department of Applied Science for Electronics and Materials,
Interdisciplinary Graduate School of Engineering Sciences,
Kyushu University, Kasuga, Fukuoka 816-8580, Japan*

Boris A. Malomed

*Department of Physical Electronics, School of Electrical Engineering,
Faculty of Engineering, Tel Aviv University, Tel Aviv 69978, Israel*

It is commonly known that two-dimensional mean-field models of optical and matter waves with the cubic self-attraction cannot produce stable solitons in free space because of the occurrence of the collapse in the same setting. By means of the numerical analysis and variational approximation, we demonstrate that the two-component model of the Bose-Einstein condensate with the spin-orbit Rashba coupling and cubic attractive interactions, gives rise to solitary-vortex complexes of two types: *semi-vortices* (SVs, with a vortex in one component and a fundamental soliton in the other), and *mixed modes* (MMs, with topological charges 0 and ± 1 mixed in both components). These two-dimensional composite modes can be created using the trapping harmonic-oscillator (HO) potential, but remain *stable* in the free space, if the trap is gradually removed. The SVs and MMs realize the ground state of the system, provided that the self-attraction in the two components is, respectively, stronger or weaker than the cross-attraction between them. The SVs and MMs which are not the ground states are subject to a drift instability. In the free space (in the absence of the HO trap), modes of both types degenerate into unstable Townes solitons when their norms attain the respective critical values, while there is no lower existence threshold for the stable modes. Moving free-space stable solitons are also found in the present non-Galilean-invariant system, up to a critical velocity. Collisions between two moving solitons lead to their merger into a single one.

I. THE MODEL

Emulation of various effects from condensed-matter physics in atomic Bose-Einstein condensates (BECs), where such effects may be studied in a simpler and clearer form, has recently attracted much attention [1]. A well-known example is the implementation of spin-orbit (SO) interactions, of both the Dresselhaus [2] and Rashba [3] types, in a binary BEC, realized experimentally [4], and elaborated in detail theoretically [5], as a mixture of two different atomic states, with a linear coupling between them induced by a specially designed laser field. In this case, the pseudo-spinor order parameter representing standard SO effects is mapped into the two-component wave functions of the mixture (a brief review of the topic was given in Ref. [6]). A similar method is also used for the emulation of gauge fields, both Abelian and non-Abelian [7], in terms of the BEC, which is a topic of a great current interest too [8].

The interplay of the SO coupling, which is a linear feature of the binary superfluid, and the mean-field BEC nonlinearity gives rise to a number of remarkable effects, such as vortices [9–11], monopoles [13] and skyrmions [14], multi-domain patterns [15], structures induced by nonlocal interactions [16], tricritical points [17], solitons [18, 19], etc. In particular, recent work [11] elaborates the description of two-dimensional (2D) vortices in trapping potentials, based on the Thomas-Fermi approximation (TFA), similar to that developed in a more general 3D setting with a spatially modulated strength of the self-repulsive nonlinearity in Ref. [12].

The use of optical lattices gives rise to additional possibilities in this context [20], including the creation of gap solitons [21]. Moreover, the fact that the system of Gross-Pitaevskii equations (GPEs), derived for the SO-coupled binary condensate in Ref. [18], is tantamount to the model of the co-propagation of orthogonal polarizations of light in twisted nonlinear optical fibers [22], establishes a link between nonlinear optical media and the SO effects in binary BEC. Another link to optics is provided by the fact that the effective pseudospin, which underlies the concept of the SO coupling in BEC, is also a central point in optical emulations of graphene [23].

While, as mentioned above, diverse vortex patterns were found in SO-coupled BEC with the repulsive nonlinearity, trapped in external potentials, the aim of the present work is to construct two-dimensional (2D) vortex solitons created in such binary condensates by *attractive* nonlinear interactions. The consideration of this setting is suggested by the accessibility of attractive interactions, usually supported by the Feshbach resonance [25], in many species of atomic BEC, including ^7Li [24], ^{85}Rb [26], Na [27], Cs [28], Cr [29], ^{39}K [30], ^{172}Yb [31], and ^{168}Er [32].

The concept of vortex solitons supported by self-attractive nonlinearities is a well-known one since the pioneering work [33], but in free space they are usually subject to strong splitting instabilities, even if the form of the nonlinearity (quadratic or saturable) prevents the onset of collapse in such media [34]. Another peculiarity of the vortex solitons

is that the simple TFA, which is efficient for handling vortices in the case of the self-repulsion, as mentioned above [11, 12], does not apply to self-attraction.

The stabilization of vortex solitons, against the collapse and splitting alike, is provided by trapping potentials, which may be spatially periodic (lattice-shaped, see reviews [35]), or harmonic-oscillator (HO) ones, as was studied in detail for the cubic [36, 37] and quadratic [38] nonlinearities. Modes with the “hidden vorticity”, i.e., two-components states with vorticities $+1$ and -1 , can also be stabilized by the harmonic-oscillator potential [37]. Although periodic potentials make the settings anisotropic, destroying the conservation of the angular momentum, the vorticity of the corresponding localized modes can be defined in the usual manner, as the phase circulation around the vortex’ pivot, divided by 2π .

The main result of the present work, reported below in Section 2, is that two different families of vortex solitons, namely *semi-vortices* (SVs, with topological charges $m = 0$ and ± 1 in the two components) and *mixed modes* (MMs, which combine $m = 0$ and ± 1 in each component) are *stable* in the 2D binary system with the Rashba coupling in the *free space*, without the support of any trapping potential. Of course, in a real experiment, any matter-wave state is created in a trapping potential. We actually demonstrate that the semi-vortices and mixed modes readily self-trap under the protection of the usual isotropic HO trapping potential, and remain stable if the potential is gradually switched off. In this connection, it is worth to mention that the SO coupling, induced by resonant laser beams [4–6], and the HO trap may be manipulated in a completely independent fashion.

The SV and MM realize, severally, the system’s ground state in the cases when the self-attraction is stronger or weaker than its cross-attraction counterpart [in terms of optics [39], these are the self-phase-modulation (SPM) and cross-phase-modulation (XPM) interactions, respectively]. Furthermore, although the Galilean invariance of the system is broken by the SO-coupling terms, stable moving modes of both SV and MM types exist too, up to a certain critical velocity, which is shown in Section 3. To the best of our knowledge, this is the first example of any species of *stable* 2D solitons in a free-space system with the attractive local cubic nonlinearity (2D solitons can be readily stabilized by nonlocal self-attraction terms [40]).

The system of 2D Gross-Pitaevskii equations (GPEs) for the spinor wave function, $\phi = (\phi_+, \phi_-)$, of the binary BEC with attractive contact interactions and the SO coupling of the Rashba type, with strength λ , which is trapped in the isotropic HO potential of strength Ω^2 , is written, in the scaled form, as

$$\begin{aligned} i\frac{\partial\phi_+}{\partial t} &= -\frac{1}{2}\nabla^2\phi_+ - (|\phi_+|^2 + \gamma|\phi_-|^2)\phi_+ + \lambda\left(\frac{\partial\phi_-}{\partial x} - i\frac{\partial\phi_-}{\partial y}\right) + \frac{1}{2}\Omega^2(x^2 + y^2)\phi_+, \\ i\frac{\partial\phi_-}{\partial t} &= -\frac{1}{2}\nabla^2\phi_- - (|\phi_-|^2 + \gamma|\phi_+|^2)\phi_- - \lambda\left(\frac{\partial\phi_+}{\partial x} + i\frac{\partial\phi_+}{\partial y}\right) + \frac{1}{2}\Omega^2(x^2 + y^2)\phi_-, \end{aligned} \quad (1)$$

where γ is the strength of the XPM interactions, while the strength of the SPM is normalized to be 1. By means of the remaining scaling freedom, we also set $\lambda = 1$. Below, stationary solutions of Eq. (1) are constructed in a numerical form, and, in parallel, by means of the variational approximation (VA, which is explicitly applied to free-space solitons, at $\Omega = 0$). Solutions for moving self-trapped modes in the free space are also obtained numerically.

To conclude the discussion of the model, it is relevant to note that the first experimental realization of the SO coupling in the binary BEC included equal strengths of the Rashba and Dresselhaus couplings [4]. However, the possibility of the experimental implementation of the Rashba coupling proper, which is assumed in Eq. (1), was elaborated in detail too [5]

II. SOLITARY VORTICAL MODES

A. Semi-vortices

First, we note that Eq. (1) admits stationary solutions in the following form:

$$\phi_+(x, y, t) = e^{-i\mu t} f_1(r^2), \quad \phi_-(x, y, t) = e^{-i\mu t + i\theta} r f_2(r^2), \quad (2)$$

where μ is the chemical potential of the self-trapped mode, (r, θ) are polar coordinates in the plane of (x, y) , and real functions $f_{1,2}(r^2)$ obey the following equations:

$$\begin{aligned} \mu f_1 + 2\left[r^2\frac{d^2 f_1}{d(r^2)^2} + \frac{df_1}{d(r^2)}\right] + (f_1^2 + \gamma r^2 f_2^2) f_1 - 2\lambda(r^2 f_2' + f_2) - \frac{1}{2}\Omega^2 r^2 f_1 &= 0, \\ \mu f_2 + 2\left[r^2\frac{d^2 f_2}{d(r^2)^2} + 2\frac{df_2}{d(r^2)}\right] + (r^2 f_2^2 + \gamma f_1^2) f_2 + 2\lambda f_1' - \frac{1}{2}\Omega^2 r^2 f_2 &= 0. \end{aligned} \quad (3)$$

These solutions are built as bound states of a fundamental soliton in component ϕ_+ (with zero topological charge, $m_+ = 0$), and a solitary vortex, with $m_- = 1$, in ϕ_- . Accordingly, composite modes of this type may be called *semi-vortices* (in Ref. [10], similar composite modes, found in a model with the repulsive nonlinearity, were called “half vortices”). The invariance of Eq. (1) with respect to the transformation,

$$\phi_{\pm}(r, \theta) \rightarrow \phi_{\mp}(r, \pi - \theta), \quad (4)$$

gives rise to a semi-vortex which is a mirror image of (2), with the pair of $(m_+ = 0, m_- = 1)$ replaced by $(m_+ = -1, m_- = 0)$:

$$\phi_+(x, y, t) = -re^{-i\mu t - i\theta} f_2(r^2), \quad \phi_- = e^{-i\mu t} f_1(r^2). \quad (5)$$

The analysis of the free-space version of Eq. (3), with $\Omega = 0$, at $r \rightarrow \infty$ shows that the respective asymptotic form of the solution is (written in terms of r , rather than r^2)

$$f_1^{(\Omega=0)} \approx Fr^{-1/2} e^{-\sqrt{-2\mu-\lambda^2}r} \cos(\lambda r + \delta), \quad f_2^{(\Omega=0)} \approx -Fr^{-3/2} e^{-\sqrt{-2\mu-\lambda^2}r} \sin(\lambda r + \delta), \quad (6)$$

where F and δ are arbitrary real constants, in terms of the asymptotic approximation. Thus, the localized modes exist at values of the chemical potential

$$\mu < -\lambda^2/2. \quad (7)$$

In fact, Eq. (6) gives the asymptotic form of the free-space solitons not only for the semi-vortices, but in the general case too.

As shown below [see Fig. 4(c), where the semi-vortex branch is labeled “0”, which implies that ϕ_+ contains solely the zero vorticity], the free-space semi-vortices represent the ground state of the system, in the absence of the trapping potential, at $\gamma \leq 1$. The coexistence of the semi-vortices in the two mutually symmetric forms, (2) and (5), implies the degeneracy of the ground state, which is possible in nonlinear systems, unlike linear ones.

Previously, composite solitons built of vortical and fundamental components were considered in a system of XPM-coupled nonlinear Schrödinger equations [41]. However, as said above, the usual system with the SPM and XPM terms cannot produce stable solitons in free space.

Stable SVs were generated, as solutions to Eq. (1) with $\gamma = 0$ (no XPM nonlinearity), by means of imaginary-time simulations [42], starting from input

$$\phi_+^{(0)} = A_1 \exp(-\alpha_1 r^2), \quad \phi_-^{(0)} = A_2 r \exp(i\theta - \alpha_2 r^2), \quad (8)$$

where $A_{1,2}$ and $\alpha_{1,2} > 0$ are real constants. Obviously, this input conforms to the general ansatz (2) for the semi-vortices. As shown in Figs. 1(a,c), to emulate an experimentally feasible scenario, the solution was constructed in this way in the presence of the HO potential, which was then slowly switched off, in real time. The SV adiabatically follows the relaxation of the HO potential, remaining dynamically stable, and eventually transforming into an SV which stays *completely stable* in the free space, with $\Omega = 0$. As said above, this is, to the best of our knowledge, the first example of stable 2D solitons in free space, supported by a local cubic self-attraction. In fact, as shown in Fig. 2(a), the SV with the same norm,

$$N = \iint (|\phi_+|^2 + |\phi_-|^2) dx dy \equiv N_+ + N_-, \quad (9)$$

can be found equally well, by means of the imaginary-time integration, directly in the free space, setting $\Omega = 0$ from the outset. It is easy to check that not only profiles $|\phi_+(x, 0)|$ and $|\phi_-(x, 0)|$ of the two field components, in the cross section of $y = 0$, which are displayed in Figs. 1(c) and 2(a), but also the entire shapes of the SVs, which are produced, severally, by the adiabatic relaxation of the trapping potential to $\Omega = 0$ in real time, and by the direct imaginary-time simulations in the free space, are virtually identical.

Further, Fig. 2(b) represents the entire family of the free-space SVs by means of their chemical potential μ , shown as a function of the norm. Note that the $\mu(N)$ dependence satisfies the Vakhitov-Kolokolov (VK) criterion [43, 44], $d\mu/dN < 0$, which is a necessary condition for the stability of solitary modes supported by the self-attractive nonlinearity, although the criterion does not secure stability of vortex solitons against splitting [35]. We stress that, as clearly seen in Fig. 2(b), there is no finite minimum (threshold) value of N necessary for the existence of the SVs in the free space.

The wave form (8) can be used not only as the input for the imaginary-time simulations, but also as a variational ansatz for the description of the free-space SVs (the VA can be extended for the model including the HO potential,

but the results are most interesting for $\Omega = 0$). Its substitution in the expression for the total energy corresponding to Eqs. (1) with $\Omega = 0$,

$$E = \int \int \left\{ \frac{1}{2} (|\nabla\phi_+|^2 + |\nabla\phi_-|^2) - \frac{1}{2} (|\phi_+|^4 + |\phi_-|^4) - \gamma|\phi_+|^2|\phi_-|^2 + \frac{\lambda}{2} \left[\phi_+^* \left(\frac{\partial\phi_-}{\partial x} - i \frac{\partial\phi_-}{\partial y} \right) + \phi_-^* \left(-\frac{\partial\phi_+}{\partial x} - i \frac{\partial\phi_+}{\partial y} \right) \right] + \text{c.c.} \right\} dx dy, \quad (10)$$

where c.c. stands for the complex conjugate, yields

$$E_{\text{semi}} = \pi \left[\frac{A_1^2}{2} - \frac{A_1^4}{8\alpha_1} + \frac{A_2^2}{2\alpha_2} - \frac{A_2^4}{64\alpha_2^3} - \frac{\gamma A_1^2 A_2^2}{4(\alpha_1 + \alpha_2)^2} + \frac{4\lambda A_1 A_2 \alpha_1}{(\alpha_1 + \alpha_2)^2} \right], \quad (11)$$

while the total norm (9) of the ansatz is $N = \pi [A_1^2/(2\alpha_1) + A_2^2/(4\alpha_2^2)]$. Then, values of amplitudes A_1, A_2 and inverse squared widths α_1, α_2 of the ansatz are predicted by the minimization of E with respect to the variational parameters, $\partial E_{\text{semi}}/\partial(A_{1,2}, \alpha_{1,2}) = 0$. These equations can be easily solved numerically. Figure 2(c) displays the comparison of the so predicted amplitude A_1 and the maximum value of $|\phi_+|$ obtained from the imaginary-time-generated solution at $\gamma = 0$. The family of the semi-vortices exists at $N < N_c \approx 5.85$, the latter value being the well-known collapse threshold for fundamental (Townes) solitons in the free 2D space [44]. Indeed, Fig. 2(d) shows, by means of the dependence of ratio N_+/N on N , that the vortical component ϕ_- vanishes at $N \rightarrow N_c$, hence in this limit the semi-vortex degenerates into the usual unstable Townes soliton, which is subject to the collapse.

In the opposite limit of $N \rightarrow 0$, the nonlinear terms in Eqs. (1) become vanishingly small, and the ground-state solution degenerates into a quasi-plane-wave with vanishing amplitudes, radial wavenumber λ and chemical potential $\mu_0 = -\lambda^2/2$, cf. Eqs. (6) and (7) [45]. In accordance with this expectation, Fig. 2(d) shows that $N_+/N \rightarrow 1/2$ at $N \rightarrow 0$. The comparison with the full numerical solutions demonstrates that Gaussian ansatz (8) is inaccurate for small N , therefore Fig. 2(c) shows a large relative discrepancy between the variational and numerical results at very small N .

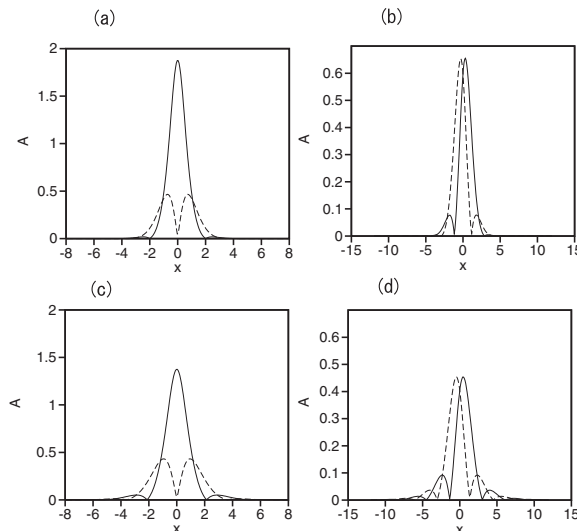


FIG. 1: (a) Cross-section profiles of the two components of a stable semi-vortex with norm $N = 5$, initiated by input (8), $|\phi_+(x, 0)|$ and $|\phi_-(x, 0)|$ (the solid and dashed curves, respectively) at $\gamma = 0, \lambda = 1$, and $\Omega = 0.5$. (b) The same for a stable mixed mode with norm $N = 2$, initiated by input (12), with $\gamma = 2, \lambda = 1$, and $\Omega = 0.5$. Both solutions, shown in (a) and (b), were generated by imaginary-time simulations. (c,d) Shapes into which the modes from panels (a,b) relax, adiabatically following the decrease of the trap's strength from $\Omega = 0.5$ to 0.

B. Mixed modes

Another type of 2D self-trapped vortical states supported by the SO-coupled model (1) can be initiated by the following input for the imaginary-time simulations, which may also serve as the variational ansatz:

$$\begin{aligned}\phi_+^{(0)} &= A_1 \exp(-\alpha_1 r^2) - A_2 r \exp(-i\theta - \alpha_2 r^2), \\ \phi_-^{(0)} &= A_1 \exp(-\alpha_1 r^2) + A_2 r \exp(i\theta - \alpha_2 r^2).\end{aligned}\quad (12)$$

States generated by this input are called MMs (mixed modes), as they are built as superpositions of states with topological charges $(0, -1)$ and $(0, +1)$ in the two components. Unlike the SVs, it is not possible to find an exact representation for these modes similar to that given by Eqs. (2) and (3), but the numerical and variational results clearly demonstrate that such states exist. Moreover, they play the role of the ground state of the system at $\gamma \geq 1$, see Fig. 4(c) below, where the mixed-mode branch is labeled “01”, as vorticities 0 and ± 1 are combined in these modes. In accordance with the form of ansatz (12), the mixed mode is transformed into itself by symmetry reflection (4).

Similar to the SVs, Figs. 1(b,d) demonstrate that stable MMs can be created under the protection of the HO potential, then adiabatically following the decrease of the potential’s strength to $\Omega = 0$, while keeping the full stability. Also similar to the SVs, Fig. 3(a) demonstrates that the so transformed MMs are identical to solutions of the same type, created directly by means of the imaginary-time integration in free space.

The $\mu(N)$ dependence for the free-space MM family is displayed in Fig. 3(b), which shows that the VK criterion holds in this case too, and, as well as SVs, the MMs do not require any finite threshold value of N necessary for their existence either. The family exists in the interval of $N < N'_c = 2N_c/(1 + \gamma)$, where N_c is the above-mentioned critical norm corresponding to the Townes solitons. Indeed, in the limit of $N \rightarrow N'_c$ the vortical components vanish in the MM, and it degenerates into the two-component Townes soliton, similar to the degeneration of the SV, cf. Figs. 2(b) and (c). In the opposite limit of $N \rightarrow 0$, the MM degenerates into a quasi-plane-wave with chemical potential $-\lambda^2/2$, which is again similar to the behavior of the SV, in the same limit.

The insertion of input (12), as the variational ansatz, into energy functional (10) yields

$$E_{\text{mixed}} = \pi \left[A_1^2 + \frac{A_2^2}{\alpha_2} - (1 + \gamma) \left(\frac{A_1^4}{4\alpha_1} + \frac{A_2^4}{32\alpha_2^3} \right) - \frac{A_1^2 A_2^2}{(\alpha_1 + \alpha_2)^2} + \frac{8\lambda A_1 A_2 \alpha_1}{(\alpha_1 + \alpha_2)^2} \right], \quad (13)$$

the total norm of the ansatz being $N = \pi [A_1^2/\alpha_1 + A_2^2/(2\alpha_2^2)]$. Numerical solution of the respective energy-minimization equations, $\partial E_{\text{mixed}}/\partial(A_{1,2}, \alpha_{1,2}) = 0$, produces values of the parameters of the variational ansatz. Figure 3(c) compares the absolute value of the fields at the central point, $|\phi_+(0, 0)|$ and its variational counterpart, $|A_1|$, as a function of the total norm.

As seen in Fig. 3(a), peak positions of components $|\phi_+(x, y)|$ and $|\phi_-(x, y)|$ in the MM are separated along x , Fig. 3(d) showing the separation (DX) as a function of the norm. For a small amplitude of the vortex component, A_2 , Eq. (12) yields $DX \approx A_2/(\alpha_1 A_1)$. The separation vanishes as N approaches the aforementioned critical value N'_c , at which the MM degenerates into the two-component Townes solitons. This is explained by the fact that, as said above, the vortical components of the wave functions, which cause the shift of the peaks from the center, vanish in this limit.

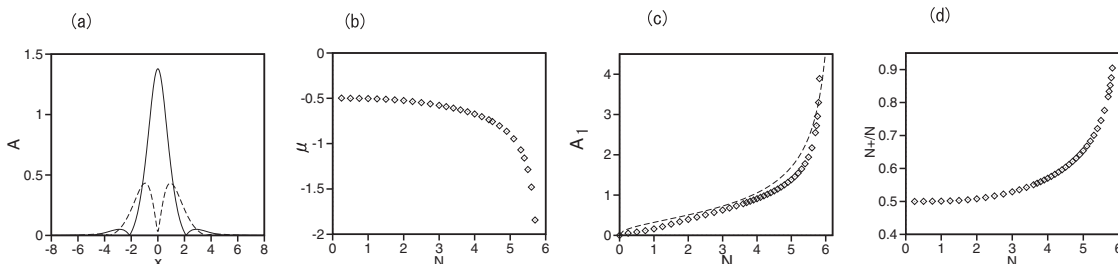


FIG. 2: Semi-vortices in the free space ($\Omega = 0$). (a) The same as in Fig. 1(a), but for the stable semi-vortex with $\Omega = 0$. (b) Chemical potential μ vs. norm N for the family of localized semi-vortices. (c) Comparison of the numerically found amplitude, $|\phi_+(0, 0)|$ (the chain of rhombuses), and A_1 , as predicted by the variational approximation (the dashed curve). (d) Ratio N_+/N as a function of N , for the family of the semi-vortices.

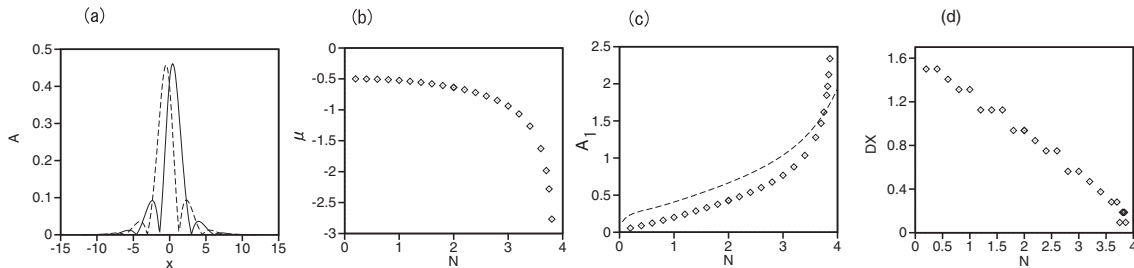


FIG. 3: Mixed modes in the free space ($\Omega = 0$). (a) The same as in Fig. 1(b), but for the stable semi-vortex with $\Omega = 0$. (b) The chemical potential of the mixed mode vs. norm N for $\gamma = 2$, $\lambda = 1$. (c) The comparison of the numerically found central amplitude of the mixed mode, $|\phi_{\pm}(0,0)|$ (the chain of rhombuses), and its variational counterpart A_1 (the dashed curve), vs. N . (d) Separation DX between peak positions of $|\phi_+|$ and $|\phi_-|$ vs N .

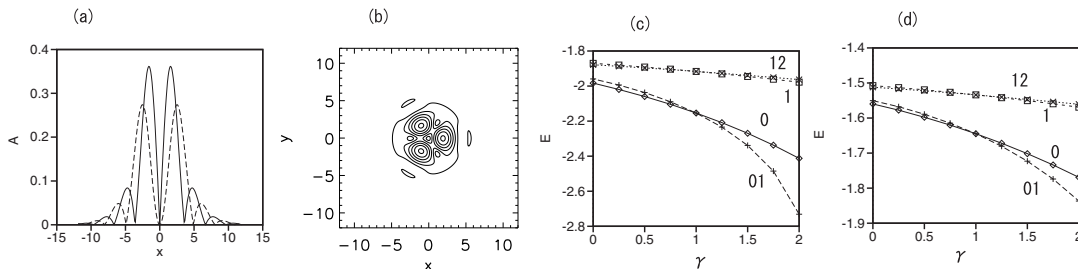


FIG. 4: (a) Cross-section profiles $|\phi_+(x,0)|$ and $|\phi_-(x,0)|$ (solid and dashed curves, respectively) for the excited state in the free space, generated by input (16) for $N = 5$ and $\lambda = 1, \gamma = 0, \Omega = 0$. (b) Contour plot of $|\phi_+(x,y)|$ for the excited state generated by input (17) for $N = 3$ and $\lambda = 1, \gamma = 2, \Omega = 0$. (c) Total energies for the four free-space stationary states, viz., the semi-vortex (labeled “0”), mixed state (“01”), and the excited states generated by inputs (16) and (17) (labeled “1” and “12”, respectively), all taken at a fixed value of the total norm, $N = 3.7$, vs. the XPM interaction constant, γ . (d) The same as in (c), but for $N = 3$.

C. Excited states

In addition to two types of the ground states, SVs and MMs, numerical analysis reveals their excited varieties. First, a set of excited states can be constructed following the general SV pattern given above by Eq. (2):

$$\phi_+(x, y, t) = e^{-i\mu t + iS\theta} r^S f_1(r^2), \quad \phi_-(x, y, t) = e^{-i\mu t + i(S+1)\theta} r^{S+1} f_2(r^2), \quad (14)$$

with integer $S \geq 1$. The substitution of this ansatz into Eq. (1) leads to a system of equations for $f_{1,2}(r^2)$:

$$\begin{aligned} \mu f_1 + 2r^2 f_1'' + 2(1+S)f_1' + r^{2S}(f_1^2 + \gamma r^2 f_2^2) f_1 - 2\lambda [r^2 f_2' + (1+S)f_2] - \frac{1}{2}\Omega^2 r^2 f_1 &= 0, \\ \mu f_2 + 2r^2 f_2'' + 2(2+S)f_2' + r^{2S}(r^2 f_2^2 + \gamma f_1^2) f_2 + 2\lambda f_1' - \frac{1}{2}\Omega^2 r^2 f_2 &= 0. \end{aligned} \quad (15)$$

In the case of $S = 0$, Eq. (15) is tantamount to Eq. (3) for the SV. Of course, mirror-image counterparts of excited states (14), generated by transformation (4), exist too.

In the numerical form, the excited state in the free space ($\Omega = 0$), corresponding to $S = 1$ in Eq. (14), was found by means of the imaginary-time integration starting with the following input:

$$\phi_+ = A_1 r e^{i\theta} e^{-\alpha_1 r^2 - i\mu t}, \quad \phi_- = A_2 r^2 e^{2i\theta} e^{-\alpha_2 r^2 - i\mu t}. \quad (16)$$

Figure 4(a) shows cross-section profiles for an example of this excited state, obtained with $N = 5$ and $\gamma = 0$. In Figs. 4(c,d), the branch of these excited-state solutions is labeled “1”, as it contains vorticity $m_+ = 1$ in component ϕ_+ .

Another type of excited states in the free space was generated by the input with combined vorticities, $m_+ = 1, -2$

and $m_- = -1, 2$, therefore it is labeled “12” in Figs. 4(c,d):

$$\begin{aligned}\phi_+ &= A_1 r e^{i\theta} e^{-\alpha_1 r^2 - i\mu t} - A_2 r^2 e^{-2i\theta} e^{-\alpha_2 r^2 - i\mu t}, \\ \phi_- &= A_1 r e^{-i\theta} e^{-\alpha_1 r^2 - i\mu t} + A_2 r e^{2i\theta} e^{-\alpha_2 r^2 - i\mu t}.\end{aligned}\quad (17)$$

This input can be also cast into the form of

$$\begin{aligned}\phi_+ &= r e^{i\theta} (A_1 e^{-\alpha_1 r^2 - i\mu t} - A_2 r^2 e^{-3i\theta} e^{-\alpha_2 r^2 - i\mu t}), \\ \phi_- &= e^{-i\theta} (A_1 e^{-\alpha_1 r^2 - i\mu t} + A_2 r^2 e^{3i\theta} e^{-\alpha_2 r^2 - i\mu t}),\end{aligned}\quad (18)$$

which implies that it includes a vortex with topological charge 1 set at $(x, y) = (0, 0)$, and three vortices with charges -1 surrounding the origin. Figure 4(b) corroborates this interpretation by means of a contour plot of $|\phi_+(x, y)|$, which features three peaks and three holes around the origin. The holes are pivots of the three above-mentioned vortices with charges -1 . The pattern is symmetric with respect to rotation by angle $2\pi/3$. The respective contour map of $|\phi_-(x, y)|$ (not shown here) is a mirror image of $|\phi_+(x, y)|$, generated by transformation (4). This solution resembles a lattice state found in Ref. [46] for the SO-coupled BEC with the self-repulsive interactions, trapped in the HO potential.

D. The identification of the ground state, and analysis of the stability of the vortical modes in the free space

The four types of the vorticity-carrying self-trapped modes, generated by inputs (2), (12), (16), and (17), respectively, in the free space ($\Omega = 0$), can be produced by the imaginary-time integration of Eq. (1) for any value of the XPM-interaction constant, γ [in addition to the two latter modes, excited states of still higher orders can be found too – e.g., those given by Eq. (14) with $S > 1$ – but they all are strongly unstable]. To identify the system’s ground state, the total energies of the four species of the vortical modes, calculated as per Eq. (10), and denoted as E_0 (for the semi-vortices), E_{01} (for the mixed mode), and E_1, E_{12} for the excited states (16) and (17), respectively, are displayed vs. γ in Figs. 4(c,d), for two fixed values of the total norm, $N = 3.7$ and $N = 3$. It is found that the energies satisfy relations $E_0 < E_{01} < E_{12} < E_1$ at $\gamma < 1$ and $E_{01} < E_0 < E_1 < E_{12}$ at $\gamma > 1$. It is seen that the semi-vortex and mixed state realize the ground state at $\gamma < 1$ and $\gamma > 1$, respectively, while the states labeled “1” and “12” are indeed excited states, separated by a wide energy gap from the competing ground-state modes. The fact that the switch of the ground states occurs at $\gamma = 1$ is not surprising, as it corresponds to the Manakov’s nonlinearity, with equal XPM and SPM coefficients, which is known to feature various degeneracies in nonlinear systems, see, e.g., Ref. [47]. It is relevant to mention that the value of γ , which is the ratio of the strengths of the XPM and SPM nonlinearity, may be readily altered by means of the Feshbach resonance [25], hence the type of the ground state may be controlled by means of this technique.

The stability of the four species of 2D self-trapped modes constructed above was studied by means of systematic numerical simulations of their perturbed evolution in the framework of Eq. (1). The results are reported here for the generic case, represented by two values of the XPM coefficient, $\gamma = 0$ and 2, and a fixed norm, $N = 3.7$. The first result is that the SV, which is the ground state at $\gamma = 0$, and the MM, which plays the same role at $\gamma = 2$, are stable against perturbations (not shown here in detail, as their stability manifests itself in an obvious way).

Next, it is interesting to test the stability of the same two species in the cases when they are *not* ground states, i.e., the SV at $\gamma = 2$, and the MM at $\gamma = 0$. In the former case, we observe in Fig. 5(a) that the SV profile keeps the initial shape from $t = 0$ till $t = 750$, which exceeds 100 diffraction times for the present mode. However, an instability manifests itself in spontaneous motion of the soliton with a nearly constant velocity, as seen in Fig. 5(b), where coordinates of the peak position of the ϕ_+ component, (X, Y) , are shown as a function of time. On top of the mean velocity, the peak features oscillatory motion with a small amplitude, see Fig. 5(c).

The evolution of the mixed mode at $\gamma = 0$, when it is not the ground state either, is shown in Fig. 6. Panels (a), pertaining to $t = 50$ and $t = 500$ (the latter can be estimated to be $\simeq 70$ diffraction times of the present mode), demonstrate that this state is unstable, starting spontaneous motion and losing the original symmetry between $|\phi_+|$ and $|\phi_-|$ with respect to transformation (4). By $t = 500$, the mixed mode rearranges into a state close to a semi-vortex. Further, Fig. 6(b) shows the time evolution of amplitudes of the ϕ_+ and ϕ_- components (the solid and dashed curves, respectively) for $0 < t < 750$. Breaking the original symmetry, the amplitude of $|\phi_+|$ increases toward the value of the amplitude of the $|\phi_+|$ component of the semi-vortex state for the same $N = 3.7$, while the amplitude of $|\phi_-|$ falls to become nearly equal to the amplitude of the $|\phi_-|$ component of the same SV. Figure 6(c) shows a trajectory of the peak position of the $|\phi_+|$ component. The localized state moves spontaneously, featuring oscillations in the x direction, while the average velocity in the y -direction is $v_y = -0.0175$.

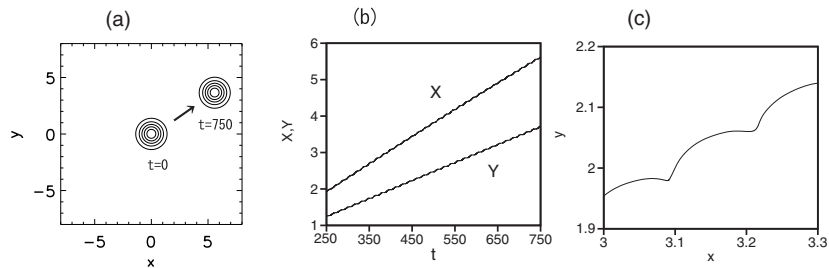


FIG. 5: (a) The evolution of the semi-vortex with $N = 3.7$, initiated by input (8) in the free space ($\Omega = 0$), at $\gamma = 2$, when the semi-vortex is *not* the ground state, according to Fig. 4(c). The contour plots of $|\phi_+(x, y)|$ at $t = 0$ and $t = 750$ are shown. (b) The time dependence of the coordinates of the peak position, (X, Y) , of $|\phi_+(x, y)|$. (c) A zoom of a segment of the trajectory $(X(t), Y(t))$, which demonstrates a small oscillatory component of the motion.

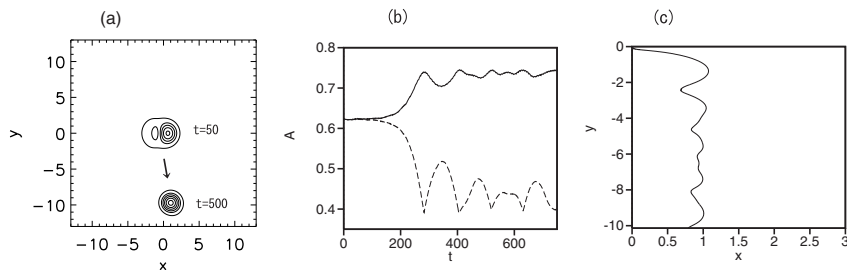


FIG. 6: (a) Contour plots of $|\phi_+(x, y)|$ at $t = 50$ and $t = 500$ for the mixed mode generated by input (12) with $N = 3.7$ in the free space ($\Omega = 0$), at $\gamma = 0$, when this mode is not a ground state. (b) The evolution of amplitudes of the ϕ_+ and ϕ_- components (solid and dashed curves, respectively) for $0 < t < 750$. (c) The trajectory of the peak position of $|\phi_+(x, y)|$ for $0 < t < 500$.

The excited states generated by inputs (16) and (17) are unstable both at $\gamma = 0$ and $g = 2$. In particular, the ring structure of the former vortical state splits in the course of the evolution, as shown in Fig. 7 for $\gamma = 0$. Similar splitting is observed much earlier (already at $t = 100$) for $\gamma = 2$.

Figure 8 illustrates the evolution of the excited state obtained from input (17) at $\gamma = 2$. The original vortex complex is broken by the instability, evolving into an apparently chaotic pattern. This instability develops quickly, as $t = 250$ [Fig. 8(c)] corresponds to $\lesssim 5$ diffraction times of the original structure.

Additional analysis (not shown here in detail) demonstrates that, in the presence of the HO trapping potential, the SV and MM remain, severally, stable at $\gamma < 1$ and $\gamma > 1$. On the other hand, although the instability of the same modes in the opposite cases, i.e., $\gamma > 1$ for the SV, and $\gamma < 1$ for the MM, manifests itself, in the free space, by spontaneous drift (see Figs. 5 and 6, respectively), additional simulations demonstrate that the confining HO potential, unless it is very tight, does not suppress the drift instability. Thus, the results obtained in the free space

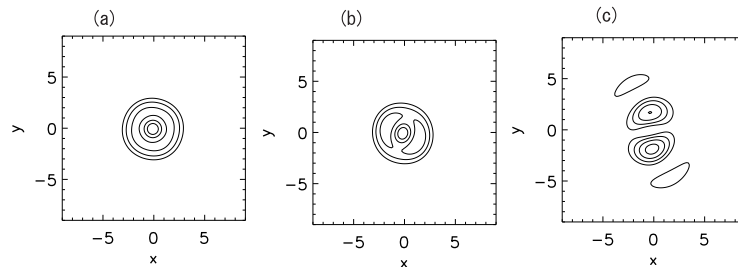


FIG. 7: Contour plot of $|\phi_+(x, y)|$ of the excited vortical state, generated by input (16) with $N = 3.7$ in the free space ($\Omega = 0$), at $\gamma = 0$: (a) $t = 500$, (b) $t = 950$, (c) $t = 1200$. At $\gamma = 2$, the instability of this excited state is essentially stronger.

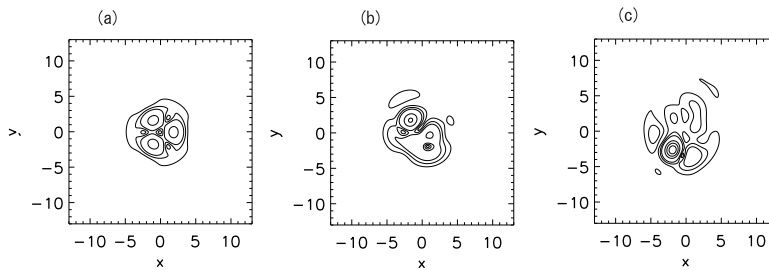


FIG. 8: Contour plot of $|\phi_+(x, y)|$ at $t = 50$ (a), $t = 150$ (b), and $t = 250$ (c) for the excited state with $N = 3.7$, generated by input (17) in the free space ($\Omega = 0$), at $\gamma = 2$. At $\gamma = 0$ this mode is unstable too.

adequately represent the situation in the presence of the HO potential too.

III. MOBILITY AND COLLISIONS OF VORTEX MODES IN THE FREE SPACE

The numerical results displayed in Figs. 5 and 6 suggest that propagating modes may exist in the free space. Localized states which move steadily at velocity $\mathbf{v} = (v_x, v_y)$ can be looked for in the form of $\phi_+ = \phi_+(x - v_x t, y - v_y t, t)$ and $\phi_- = \phi_-(x - v_x t, y - v_y t, t)$. The substitution of this into Eq. (1) with $\Omega = 0$ leads to the equations written in the moving reference frame,

$$\begin{aligned} i\frac{\partial\phi_+}{\partial t} - i(\mathbf{v} \cdot \nabla)\phi_+ &= -\frac{1}{2}\nabla^2\phi_+ - (|\phi_+|^2 + \gamma|\phi_-|^2)\phi_+' + \lambda\left(\frac{\partial\phi_-}{\partial x} - i\frac{\partial\phi_-}{\partial y}\right), \\ i\frac{\partial\phi_-}{\partial t} - i(\mathbf{v} \cdot \nabla)\phi_- &= -\frac{1}{2}\nabla^2\phi_- - (|\phi_-|^2 + \gamma|\phi_+|^2)\phi_-' + \lambda\left(-\frac{\partial\phi_+}{\partial x} - i\frac{\partial\phi_+}{\partial y}\right), \end{aligned} \quad (19)$$

where x and y actually stand for $x - v_x t$ and $y - v_y t$. Note that Eq. (1) has no Galilean invariance, hence steadily propagating solutions cannot be generated by a straightforward transformation, such as

$$\phi_{\pm}(\mathbf{r}) \equiv \tilde{\phi}_{\pm}(\mathbf{r}) \exp\left(i\mathbf{v} \cdot \mathbf{r} - \frac{i}{2}v^2 t\right). \quad (20)$$

In particular, in the case of $v_x = 0$ (in this case, solutions for moving modes exist, as shown below), the quasi-Galilean transformation (20) casts Eq. (19) into a form which differs from underlying equations (1) by the presence of terms causing for linear mixing of the two components:

$$\begin{aligned} i\frac{\partial\phi_+}{\partial t} &= -\frac{1}{2}\nabla^2\phi_+ - (|\phi_+|^2 + \gamma|\phi_-|^2)\phi_+' + \lambda\left(\frac{\partial\phi_-}{\partial x} - i\frac{\partial\phi_-}{\partial y}\right) + \lambda v_y \phi_-, \\ i\frac{\partial\phi_-}{\partial t} &= -\frac{1}{2}\nabla^2\phi_- - (|\phi_-|^2 + \gamma|\phi_+|^2)\phi_-' + \lambda\left(-\frac{\partial\phi_+}{\partial x} - i\frac{\partial\phi_+}{\partial y}\right) + \lambda v_y \phi_+. \end{aligned} \quad (21)$$

The same linear mixing can be imposed, in diverse 1D [48] and 2D [49] settings, by a GHz wave coupling the two underlying atomic states, i.e., the linear mixing by itself represents a physically relevant addition to the basic model. A straightforward impact of the addition of the mixing terms in Eq. (21) is a shift of the edge of the *semi-infinite gap* (7) in which solitons may exist, from $\mu = -\lambda^2/2$ to $\mu < -(\lambda^2/2 + |\lambda v_y|)$.

Coming back to equations (19) written in the moving reference frame, stationary solutions to these equations can be obtained, as well as in the case of underlying equations (1), by means of the imaginary-time evolution method for $v_y \neq 0$, but the procedure produces results solely for $v_x = 0$ (this situation is possible, as the present 2D system is not isotropic). In particular, at $\gamma = 2$, when the quiescent MM is the ground state, its moving version, which is displayed in Figs. 9(a,b) for $N = 3.1$ and $v_y = 0.5$, exists and is stable too. As well as its quiescent counterpart, this mode features the mirror symmetry between the profiles of $|\phi_+(x, y)|$ and $|\phi_-(x, y)|$. Figure 9(c) shows the amplitude of the moving MM, $A = \sqrt{|\phi_+(x=0, y=0)|^2 + |\phi_-(x=0, y=0)|^2}$, as a function of v_y . The amplitude monotonously decreases with the growth of the velocity, and the mode vanishes at $v_y = (v_y)_{\max}^{(\text{mixed})} \approx 1.8$.

The availability of the stably moving mixed modes suggests to consider collisions between them. In particular, we have performed simulations of Eq. (1) for the head-on collision between two solitons displayed in Figs. 9(a,b), moving

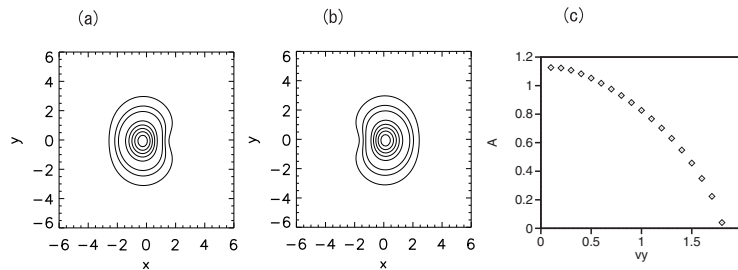


FIG. 9: Contour plots of $|\phi_+(x,y)|$ (a) and $|\phi_-(x,y)|$ of the stable mixed mode with norm $N = 3.1$, moving at velocity $v_y = 0.5$ (while $v_x = 0$) in the free space ($\Omega = 0$), for $\gamma = 2, \lambda = 1$. (c) The amplitude of the moving mixed mode as a function of v_y , also for $N = 3.1$.

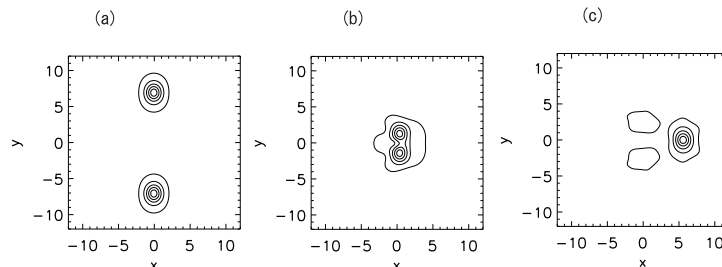


FIG. 10: The head-on collision between two mixed-mode solitons with norms $N = 3.1$ moving, in the free space ($\Omega = 0$), at velocities $v_y = \pm 0.5$ [the same as those shown in Fig. 9(a,b)]. Contour plots of $\sqrt{|\phi_+(x,y)|^2 + |\phi_-(x,y)|^2}$ are displayed at $t = 4$ (a), $t = 24$ (b), and $t = 64$ (c).

at velocities $v_y = \pm 0.5$. Figures 10(a), (b), and (c) display snapshot patterns of $\sqrt{|\phi_+(x,y)|^2 + |\phi_-(x,y)|^2}$ at $t = 4$, $t = 24$, and $t = 64$, respectively. The collision results in fusion of the two solitons into a single state, of the same MM type, which is spontaneously drifting along direction x with velocity $v_x \approx 0.14$. The drift may be understood as a manifestation of spontaneous symmetry breaking caused by the collision. Strictly speaking, this state, produced by the fusion, is not a steadily moving one, because, as mentioned above, the imaginary-time integration of Eq. (19) does not produce MM solitons moving in the direction of x . The fusion is accompanied by emission of small-amplitude radiation waves.

At $\gamma = 0$, the SV, which, as shown above, is the ground state in the class of quiescent modes in this case, can also move stably, but only in a small interval of velocities,

$$|v_y| \leq (v_y)_{\max}^{(\text{semi})} \approx 0.03 \quad (22)$$

[cf. a much larger velocity found above for the moving MM at $\gamma = 2$]. Figures 11(a) and (b) show the profiles of $|\phi_+(x,y)|$ and $|\phi_-(x,y)|$ for the SV with norm $N = 3.7$, moving at velocity $v_y = -0.02$. In addition, Fig. 11(c) displays the evolution of $\sqrt{|\phi_+|^2 + |\phi_-|^2}$ in the cross section of $x = 0$, produced by direct simulations of Eq. (1), starting from the initial conditions corresponding to Figs. 11(a,b). The localized solution is stably moving at velocity $v_y = -0.02$. In fact, this moving state is similar to the one generated by the spontaneous onset of motion of the unstable quiescent MM at $\gamma = 0$ and the same norm, which rearranges into a state close to the SV, as shown above in Fig. 6.

At $|v_y| > 0.03$ [see Eq. (22)], the solution to Eq. (19) produced by means of the imaginary-time-propagation method converges not to an SV, but rather to an MM state, which turns to be stable in real-time simulations. Thus, the moving SVs are rather fragile objects, while the MMs are, on the contrary, very robust ones in the state of motion.

IV. CONCLUSIONS

The objective of this work was to construct several types of self-trapped vortex-soliton complexes in the 2D model of the binary BEC, with the SO coupling of the Rashba type between the two components and attractive intrinsic

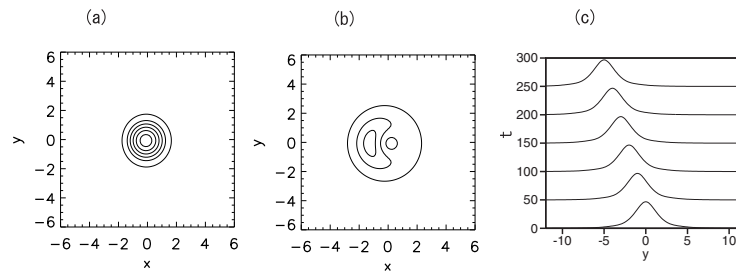


FIG. 11: Contour plots of $|\phi_+(x, y)|$ (a) and $|\phi_-(x, y)|$ for the stable semi-vortex with norm $N = 3.7$, which moves, in the free space ($\Omega = 0$), at velocity $v_y = -0.02$. (c) The evolution of $\sqrt{|\phi_+(0, y)|^2 + |\phi_-(0, y)|^2}$ in the cross section drawn through $x = 0$.

nonlinearity. The most essential finding is that, on the contrary to the commonly known instability of 2D free-space solitons and vortices in previously studied models with the attractive cubic terms, two species of *stable* modes have been found here in the numerical form and by means of the VA (variational approximation), *viz.*, the SVs (semi-vortices) and MMs (mixed modes), which represent the system's ground state when the SPM attraction is, respectively, stronger or weaker than its XPM counterpart. An experimentally relevant scenario was elaborated, which assumes that the SVs and MMs are originally created under the protection of the HO trapping potential, which is subsequently switched off, slowly enough. The stable modes readily follow the lifting of the trap, adiabatically carrying over into the stable self-trapped states which exist in the free space.

The general structure of the SVs and similar higher-order excited states was found in the exact form, see Eqs. (2), (3) and (14), (15). In the free space, the SVs and MMs turn into the commonly known unstable Townes solitons when norms of these states approach the corresponding limit values, while there is no lower threshold value of the norm necessary for their existence. Moving stable modes have been found too, up to the respective critical velocities, in spite of the lack of the Galilean invariance in the system. Collisions between moving mixed modes lead to their fusion.

It should be relevant to extend the analysis by including a spatially periodic potential (rather than the HO potential considered here). Another interesting generalization is to introduce the “nonlinearity management” [50], that would periodically (in time) switch the system between regions of $\gamma < 1$ and $\gamma > 1$, where the two different types of the ground states are expected, *viz.*, the SVs and MMs, respectively. The periodic switching between them may give rise to new dynamical regimes.

-
- [1] P. Hauke, F. M. Cucchietti, L. Tagliacozzo, I. Deutsch, and M. Lewenstein, Rep. Prog. Phys. **75**, 082401 (2012).
[2] G. Dresselhaus, Phys. Rev. **100**, 580 (1955).
[3] Y. A. Bychkov and E. I. Rashba, J. Phys. C **17**, 6039 (1984).
[4] Y. J. Lin, K. Jimenez-Garcia, and I. B. Spielman, Nature **471**, 83 (2011).
[5] Y. Zhang, L. Mao, and C. Zhang, Phys. Rev. Lett. **108**, 035302 (2012).
[6] H. Zhai, Int. J. Mod. Phys. B **26**, 1230001 (2012).
[7] Y.-J. Lin, R. L. Compton, A. R. Perry, W. D. Phillips, J. V. Porto, and I. B. Spielman, Phys. Rev. Lett. **102**, 130401 (2009); Y.-J. Lin, R. L. Compton, K. Jiménez-García, J. V. Porto, and I. B. Spielman, Nature **462**, 628 (2009); T.-L. Ho and S. Zhang, Phys. Rev. Lett. **107**, 150403 (2011).
[8] J. Dalibard, F. Gerbier, G. Juzeliūnas, and P. Öhberg, Rev. Mod. Phys. **83**, 1523 (2011); N. Goldman, G. Juzeliūnas, P. Öhberg, and I. B. Spielman, arXiv:1308.6533v1.
[9] C. J. Wu, Mod. Phys. Lett. B **23**, 1 (2009); X.-Q. Xu and J. H. Han, Phys. Rev. Lett. **107**, 200401 (2011); T. Kawakami, T. Mizushima, and K. Machida, Phys. Rev. A **84**, 011607 (2011); J. Radić, T. A. Sedrakyan, I. B. Spielman, and V. Galitski, *ibid.* **84**, 063604 (2011); X.-F. Zhou, J. Zhou, and C. Wu, *ibid.* **84**, 063624 (2011); Z. F. Xu, Y. Kawaguchi, L. You, and M. Ueda, *ibid.* A **86**, 033628 (2012); E. Ruokokoski, J. A. M. Huhtamaki, and M. Mottonen, *ibid.* **86**, 051607 (2012); H. Sakaguchi and B. Li, *ibid.* **87**, 015602 (2013).
[10] B. Ramachandhran, B. Opanchuk, X.-J. Liu, H. Pu, P. D. Drummond, and H. Hu, *ibid.* **85**, 023606 (2012).
[11] A. L. Fetter, Phys. Rev. A **89**, 023629 (2014); see also: A. L. Fetter, Rev. Mod. Phys. **81**, 647 (2009).
[12] R. Driben, Y. V. Kartashov, B. A. Malomed, T. Meier, and L. Torner, Phys. Rev. Lett. **112**, 020404 (2014).
[13] G. J. Conduit, Phys. Rev. A **86**, 021605(R) (2012).
[14] C. J. Wu, I. Mondragon-Shem, and X.-F. Zhou, Chin. Phys. Lett. **28**, 097102 (2011); T. Kawakami, T. Mizushima, M. Nitta, and K. Machida, Phys. Rev. Lett. **109**, 015301 (2012); C.-F. Liu and W. M. Liu, Phys. Rev. A **86**, 033602 (2012); X. F. Zhou, Y. Li, Z. Cai, and C. J. Wu, J. Phys. B: At. Mol. Opt. Phys. **46**, 134001 (2013).

- [15] C. Wang, C. Gao, C.-M. Jian, and H. Zhai, *Phys. Rev. Lett.* **105**, 160403 (2010); D. A. Zezyulin, R. Driben, V. V. Konotop, and B. A. Malomed, *Phys. Rev. A* **88**, 013607 (2013).
- [16] S. Sinha, R. Nath, and L. Santos, *Phys. Rev. Lett.* **107**, 270401 (2011); Y. Deng, J. Cheng, H. Jing, C. P. Sun, and S. Yi, *ibid.* **108**, 125301 (2012).
- [17] Y. Li, L. P. Pitaevskii, and S. Stringari, *Phys. Rev. Lett.* **108**, 225301 (2012).
- [18] V. Achilleos, D. J. Frantzeskakis, P. G. Kevrekidis, and D. E. Pelinovsky, *Phys. Rev. Lett.* **110**, 264101 (2013).
- [19] Y. Xu, Y. Zhang, and B. Wu, *Phys. Rev. A* **87**, 013614 (2013); L. Salasnich, and B. A. Malomed, *ibid.* **87**, 063625 (2013).
- [20] W. Han, S. Zhang, and W.-M. Liu, arXiv:1211.2097v3 (2013).
- [21] Y. V. Kartashov, V. V. Konotop, and F. Kh. Abdullaev, *Phys. Rev. Lett.* **111**, 060402 (2013).
- [22] B. A. Malomed, *Phys. Rev. A* **43**, 410 (1991).
- [23] M. Rechtsman, J. M. Zeuner, A. Tünnermann, S. Nolte, M. Segev, and A. Szameit, *Nature Phot.* **7**, 153 (2013); M. Rechtsman, J. M. Zeuner, Y. Plotnik, Y. Lumer, D. Podolsky, F. Dreisow, S. Nolte, M. Segev, and A. Szameit, *Nature* **496**, 196 (2013).
- [24] C. C. Bradley, C. A. Sackett, and R. G. Hulet, *Phys. Rev. Lett.* **78**, 985 (1997).
- [25] C. Chin, R. Grimm, P. Julienne, and E. Tiesinga, *Rev. Mod. Phys.* **82**, 1225 (2010).
- [26] Ph. Courteille, R. S. Freeland, and D. J. Heinzen, F. A. van Abeelen, and B. J. Verhaar, *Phys. Rev. Lett.* **81**, 69 (1998); J. L. Roberts, N. R. Claussen, J. P. Burke, Jr., C. H. Greene, E. A. Cornell, and C. E. Wieman, *ibid.* **81**, 5109 (2000).
- [27] S. Inouye, M. R. Andrews, J. Stenger, H. J. Miesner, D. M. Stamper-Kurn, and W. Ketterle, *Nature* **392**, 151 (1998); J. Stenger, S. Inouye, M. R. Andrews, H. J. Miesner, D. M. Stamper-Kurn, and W. Ketterle, *Phys. Rev. Lett.* **82**, 2422 (1999).
- [28] V. Vuletić, A. J. Kerman, C. Chin, and S. Chu, *Phys. Rev. Lett.* **82**, 1406 (1999).
- [29] A. Griesmaier, J. Stuhler, T. Koch, M. Fattori, T. Pfau, and S. Giovanazzi, *Phys. Rev. Lett.* **97**, 250402 (2006).
- [30] C. D'Errico, M. Zaccanti, M. Fattori, G. Roati, M. Inguscio, G. Modugno, and A. Simoni, *New J. Phys.* **9**, 223 (2007).
- [31] K. Enomoto, K. Kasa, M. Kitagawa, and Y. Takahashi, *Phys. Rev. Lett.* **101**, 203201 (2008).
- [32] K. Aikawa, A. Frisch, M. Mark, S. Baier, A. Rietzler, R. Grimm, and F. Ferlaino, *Phys. Rev. Lett.* **108**, 210401 (2012).
- [33] V. I. Kruglov, Y. A. Logvin, and V. M. Volkov, *J. Mod. Opt.* **39**, 2277 (1992).
- [34] W. J. Firth and D. V. Skryabin, *Phys. Rev. Lett.* **79**, 2450 (1997); L. Torner and D. V. Petrov, *Electr. Lett.* **33**, 608 (1997); D. V. Petrov, L. Torner, J. Martorell, R. Vilaseca, J. P. Torres, and C. Cojocar, *Opt. Lett.* **23**, 1787 (1998).
- [35] B. A. Malomed, D. Mihalache, F. Wise, and L. Torner, *J. Opt. B: Quant. Semicl. Opt.* **7**, R53 (2005); Y. V. Kartashov, B. A. Malomed, and L. Torner, *Rev. Mod. Phys.* **83**, 247 (2011).
- [36] F. Dalfovo and S. Stringari, *Phys. Rev. A* **53**, 2477 (1996); R. J. Dodd, *J. Res. Natl. Inst. Stand. Technol.* **101**, 545 (1996); T. J. Alexander and L. Bergé, *Phys. Rev. E* **65**, 026611 (2002); L. D. Carr and C. W. Clark, *Phys. Rev. Lett.* **97**, 010403 (2006); D. Mihalache, D. Mazilu, B. A. Malomed, and F. Lederer, *Phys. Rev. A* **73**, 043615 (2006); L. D. Carr and C. W. Clark, *ibid.* **74**, 043613 (2006); G. Herringer, L. D. Carr, R. Carretero-González, P. G. Kevrekidis, and D. J. Frantzeskakis, *ibid.* **77**, 023625 (2008).
- [37] M. Brtko, A. Gammal, and B. A. Malomed, *Phys. Rev. A* **82**, 053610 (2010).
- [38] H. Sakaguchi and B. A. Malomed, *J. Opt. Soc. Am. B* **29**, 2741 (2012).
- [39] Y. S. Kivshar and G. P. Agrawal, *Optical Solitons: From Fibers to Photonic Crystals* (Academic Press, San Diego, 2003).
- [40] S. Skupin, O. Bang, D. Edmundson, and W. Królikowski, *Phys. Rev. E* **73**, 066603 (2006).
- [41] Z. H. Musslimani, M. Segev, D. N. Christodoulides, and M. Soljačić, *Phys. Rev. Lett.* **84**, 1164 (2000); Z. H. Musslimani, M. Soljačić, M. Segev, and D. N. Christodoulides, *Phys. Rev. E* **63**, 066608 (2001).
- [42] M. L. Chiofalo, S. Succi, and M. P. Tosi, *Phys. Rev. E* **62**, 7438 (2000); D. L. Feder, M. S. Pindzola, L. A. Collins, B. I. Schneider, and C. W. Clark, *Phys. Rev. A* **62**, 053606 (2000).
- [43] M. Vakhitov and A. Kolokolov, *Radiophys. Quant. Electron.* **16**, 783 (1973).
- [44] L. Bergé, *Phys. Rep.* **303**, 259 (1998); E. A. Kuznetsov and F. Dias, *ibid.* **507**, 43 (2011).
- [45] H. Zhai, *Int. J. Mod. Phys. B* **26**, 1230001 (2012).
- [46] H. Hu, B. Ramachandhran, H. Pu, and X.-J. Liu, *Phys. Rev. Lett.* **108**, 010402 (2012).
- [47] T. Kanna, M. Vijayajayanthi, and M. Lakshmanan, *J. Phys. A: Math. Theor.* **43**, 434018 (2010); A. Mecozzi, C. Antonelli, and M. Shtaif, *Opt. Exp.* **20**, 11673 (2012).
- [48] R. J. Ballagh, K. Burnett, and T. F. Scott, *Phys. Rev. Lett.* **78**, 1607 (1997); J. Williams, R. Walser, J. Cooper, E. Cornell, and M. Holland, *Phys. Rev. A* **59**, R31 (1999); P. Öhberg and S. Stenholm, *ibid.* **59**, 3890 (1999); D. T. Son and M. A. Stephanov, *ibid.* **65**, 063621 (2002); S. D. Jenkins and T. A. B. Kennedy, *ibid.* **68**, 053607 (2003); A. Kuklov, N. Prokof'ev, and B. Svistunov, *ibid.* **69**, 025601 (2004); Q.-H. Park and J. H. Eberly, *ibid.* **70**, 021602(R) (2004); I. M. Merhasin, B. A. Malomed, and R. Driben, *J. Phys. B: At. Mol. Opt. Phys.* **38**, 877 (2005); S. K. Adhikari and B. A. Malomed, *Phys. Rev. A* **79**, 015602 (2009).
- [49] H. Saito, R. G. Hulet, and M. Ueda, *Phys. Rev. A* **76**, 053619 (2007); H. Susanto, P. G. Kevrekidis, B. A. Malomed, and F. Kh. Abdullaev, *Phys. Lett. A* **372**, 1631 (2008).
- [50] B. A. Malomed, *Soliton Management in Periodic Systems* (Springer: New York, 2006).